Kanazawa, V. Lee, P. Pfluger, J. C. Scott, and G. Weiser, *Mol. Cryst. Liq. Cryst.*, **83,** 253 (1982).
11. A. J. Downard and D. Pletcher, *J. Electroanal. Chem.*, **206,** 139 (1986).
12. F. Beck and M. Oberst, Bunsentagung 1988 Passau, Poster P167.
13. A. F. Diaz and J. I. Castillo, *J. Chem. Soc., Chem. Commun.*, 397 (1980).
14. F. Beck, M. Oberst, and P. Braun, DECHEMA-Monogr., **109,** 457 (1987).
15. F. Beck, *Electrochim. Acta*, **33,** 839 (1988).
16. J. Heinze, M. Dietrich, and J. Mortensen, *Makromol. Chem., Macromol. Symp.*, **8,** 73 (1987).
17. P. A. Christensen, A. Hamnett, and A. R. Hillman, *J. Electroanal. Chem.*, **242,** 47 (1988).
18. C. K. Baker and J. R. Reynolds, *ibid.*, **251,** 307 (1988).
19. P. Novák, P. A. Christensen, T. Iwasita, and W. Vielstich, *ibid.*, **263,** 37 (1989).
20. P. Novák and W. Vielstich, *This Journal*, Submitted.
21. See, *e.g.*, T. A. Skotheim, Editor, "Handbook of Conducting Polymers," Marcel Dekker, New York and Basel (1986), and references therein.
22. P. A. Christensen, Private communication, July 1988.
23. S. W. Feldberg, *J. Am. Chem. Soc.*, **106,** 4671 (1984).
24. J. Heinze and M. Dietrich, in Proc. of the Int. Autumn School, Electrochemistry of Conductive Polymers, Sulejow, Poland, 1988, p. 30.
25. G. B. Street, in "Handbook of Conducting Polymers," Vol. 1, T. A. Skotheim, Editor, p. 280, Marcel Dekker, New York and Basel (1986).
26. S. I. Yaniger and D. W. Vidrine, *Appl. Spectrosc.*, **40,** 174 (1986).
27. H. Kuzmany, N. S. Sariciftci, H. Neugebauer, and A. Neckel, *Phys. Rev. Lett.*, **60,** 212 (1988).

A Thermodynamic and Kinetic Study of Electrochemical Lithium Intercalation in $Na_{0.33}V_2O_5$ Bronze Prepared by a Sol-Gel Process

S. Bach

Laboratoire de Chimie de la Matière Condensée, C.N.R.S. UA 302 ENSCP, Paris, France

J. P. Pereira-Ramos

Laboratoire d'Electrochimie, Catalyse et Synthèse Organique, C.N.R.S. UM 28, 94320 Thais, France

N. Baffier

Laboratoire de Chimie de la Matière Condensée, C.N.R.S. UA 302 ENSCP, Paris, France

R. Messina

Laboratoire d'Electrochimie, Catalyse et Synthèse Organique, C.N.R.S. UM 28, 94320 Thais, France

ABSTRACT

Thermodynamic and kinetic investigations on the electrochemical lithium intercalation into β $Na_{0.33}V_2O_5$ synthesized by a sol-gel process (SGP) have been found to correlate well with the scheme suggested for the filling of the available sites M of the β structure by Li^+ ions. Indeed, the whole of the thermodynamic, kinetic, and crystallographic data have enabled one to explain the electrochemical behavior exhibited by the SGP bronze $Na_{0.33}V_2O_5$ in a lithium ion containing non-aqueous solvent. The partial molar quantities $\Delta\bar{G}_{Li(x)}$, $\Delta\bar{H}_{Li(x)}$, and $\Delta\bar{S}_{Li(x)}$ were obtained from EMF-temperature measurements and coulometric titration curves. Two main ordering processes were seen to take place in the composition range $0 < x < 0.3$ and $0.3 < x < 0.7$ in $Li_xNa_{0.33}V_2O_5$. The chemical diffusion coefficient of lithium was found to be proportional to the number of the vacant sites; $\tilde{D}_{Li}$ varies from 10^{-9} up to 10^{-12} $cm^2\ s^{-1}$ for $0 < x < 0.7$ and is in the order 10^{-14} for higher Li contents. Finally, the better electrochemical behavior of the SGP bronze β $Na_{0.33}V_2O_5$, as compared with that exhibited by the similar bronze obtained through solid-state reactions at 700°C highlighted the advantage of the sol-gel technique for the synthesis of new cathodic intercalation materials usable in secondary lithium cells.

Electrochemical lithium insertion into the vanadium bronze β $Na_{0.33}V_2O_5$ synthesized by a sol-gel process (SGP bronze) has been discussed in a previous work in terms of crystallographic data (1). Chronopotentiometric and voltammetric measurements performed in molten dimethylsulfone ($DMSO_2$) at 150°C evidenced three well-defined processes in the potential range 3.5V/2V *vs.* Li/Li^+. Taking the separation of all the sites M-M in the tunnel structure of the vanadium bronze and x-ray experiments into account, the first two steps have been correlated, respectively, with the half-occupancy of the tetrahedral and of the eight coordinated sites whereas the third one has been ascribed to the filling of all the available remaining sites.

In addition, we have shown that the synthesis of the vanadium bronze β $Na_{0.33}V_2O_5$ via a sol-gel process (SGP bronze) led to the formation of a "new bronze" in that, its structural anisotropy was found to be strongly enhanced. Indeed, x-ray diffraction experiments have revealed a preferred orientation corresponding to an alignment of the tunnels of the structure over larger domains along their common direction.

Such a feature has been clearly emphasized and results in an important improvement of the overall electrochemical behavior of the material, as compared to that of the similar bronze synthesized by a conventional solid-state reaction at high temperature (SSR bronze). In particular, the cycling behavior exhibited by the SGP bronze $Na_{0.33}V_2O_5$ at room temperature makes this compound a promising cathodic material for secondary lithium cells (1).

In the present work, more information about electrochemical lithium insertion into the β $Na_{0.33}V_2O_5$ bronze synthesized by a sol-gel process is provided. The thermodynamic and kinetic properties of the lithium intercalation reaction into the host lattice are investigated by potentiometric measurements coupled with coulometric titrations. These results are related to the main characteristics of the material.

Experimental

Synthesis of the $Na_{0.33}V_2O_5$ bronze via a sol-gel process.— The starting material is the xerogel V_2O_5 1.6 H_2O whose

preparation has been extensively described (2, 3). This compound exhibits a layered structure with a basic distance of 11.5Å. An ion exchange procedure performed in an NaCl aqueous solution allows, in the case of a total reaction, to obtain the sodium xerogel whose formula is $Na_{0.33}V_2O_5$ 1.6 H_2O and corresponds to a spacing of 10.9Å (4, 5). The latter gives rise to the formation of the vanadium bronze β $Na_{0.33}V_2O_5$ after evaporation of the water molecules at moderate temperatures (550°C). The final material consists of platelets of 0.1 mm thick. The SGP bronze structure is monoclinic (1) with the following parameters, $a = 10.10 + 0.05$Å; $b = 3.63 + 0.01$Å; $c = 15.45 + 0.05$Å; $\beta = 110° + 0.5°$, close to those of the SSR bronze (6). But x-ray diffraction experiments show that the Bragg peaks 002, 004, 104, and 106 correspond to noticeable intensities which reveals a preferred orientation of the tunnel structure parallel to the *a-b* plane. In the same way, electrical conductivity of the SGP bronze is highly anisotropic, giving values of $\sigma_{/\!/} \simeq 2\ \Omega^{-1}\ cm^{-1}$ and $\sigma_{\perp} \simeq 2 \cdot 10^{-3}\ \Omega^{-1}\ cm^{-1}$ at room temperature.

Electrochemical measurements.—Electrolytes.—Propylene carbonate (twice distilled) was obtained from Fluka and used as received. Anhydrous lithium perchlorate was dried under vacuum at 200°C for 12h. The electrolytes were prepared under a purified argon atmosphere.

Experimental technique.—The working electrode consisted of either a stainless steel or a gold grid on which the β $Na_{0.33}V_2O_5$ bronze, mixed with graphite (90% by weight graphite) or without graphite, was pressed. Such a treatment did not induce a loss of anisotropy of the SGP bronze. Lithium was used as the reference and auxiliary electrodes. The electrochemical cell has already been described (7). It was thermostated with silicone oil whose temperature (∓ 0.5°C) and circulation were controlled by a Huber T200 thermostat.

Thermodynamic and kinetic measurements were carried out in reversible galvanic cells (A)

$Li_xNa_{0.33}V_2O_5$/1*M* $LiClO_4$ in PC/Li/1*M* $LiClO_4$ in PC/Li

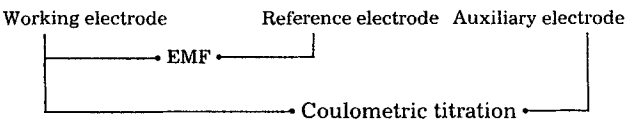

EMF temperature measurements.—The working composition was changed by coulometric titration. Reaching equilibrium after coulometric titration required a few hours at constant temperature in order to obtain a uniform Li^+ ion distribution throughout the working electrode. For $x > 0.7$ one or two days were required to reach equilibrium. Once equilibrium was reached, however, alteration to the EMF equilibrium rapidly followed any change in temperature introduced thereafter (≃30 min). Equilibrium was considered to have been reached when the open-circuit voltage remained stable (± 1 mV) for 12h, and the EMF-*T* measurements were completely reproducible after an increase or a decrease in temperature.

Results and Discussion

Typical cyclic voltammograms of $Na_{0.33}V_2O_5$ (SGP) electrodes as a function of the cutoff voltage are presented in Fig. 1. Three main processes for Li insertion and extraction in the bronze are clearly pointed out at 3.3, 2.8, and 2.5V. In all cases, and whatever the scanning rate, the amount of electricity required for the reduction and recovered in the oxidation is practically similar. Closely related sweep curves have also been obtained in the case of lithium insertion into the monoclinic lithium vanadium bronze $Li_xV_2O_5$ synthesized at high temperature (8). Within experimental error, no significant shift of the peak potentials (I) and (II) is found (from 20 up to 40 mV for sweep rates in the range $3.3 \cdot 10^{-4}/3.3 \cdot 10^{-5}\ Vs^{-1}$). Therefore, the first two steps can be considered as reversible redox processes. Nevertheless, the shoulder evidenced in the cathodic and anodic peaks of the first insertion process, and reproducible at all sweep rates, suggests that this step is subdivided into two processes.

Electrochemical lithium insertion into the β $Na_{0.33}V_2O_5$ bronze can be described according to the following reaction

$$Na_{0.33}V_2O_5 + xe^- + xLi_{el}^+ \rightleftharpoons Li_xNa_{0.33}V_2O_5$$

where the subscript el refers to the lithium ions in the electrolyte.

The redox system involved in this reaction is the vanadium couple V^V/V^{IV} located in the host lattice (9) and x is the degree of insertion of lithium in the bronze. Hence, the thermodynamic equation for the equilibrium electrode potential (E) can be given in a first approach, by the relation (1)

$$E = E^\circ_{(V^V/V^{IV}, Li^+)} + \frac{RT}{F} \ln |Li^+|_{el} + \frac{RT}{F} \ln \frac{x_{max} - x}{x} \quad [1]$$

where $x_{max} - x$ and x are the molar fractions of the V^V and (V^{IV}, Li^+) species in the $Li_xNa_{0.33}V_2O_5$ bronze, *i.e.*, the molar fractions of vacant and occupied sites M, respectively. $x_{max} = 1.6$ (1), and E° is the potential of the (V^V/V^{IV}, Li^+) couple in the bronze for the standard condition $x = 0.5\ x_{max}$.

The potential dependence of the electrochemically lithiated bronze for $x = 0.2$ has been compared with that of a metallic lithium electrode as a function of Li^+ concentration in the electrolyte. Experimental results are reported in Fig. 2. The same linear variation of E *vs.* log $|Li^+|_{el}$ was found for both redox systems, as expected from the Nernst's relation [1]. Nevertheless, the experimental values of the slopes (80 mV per log $|Li^+|_{el}$ unit) are not in accordance with the theoretical value given in Eq. [1] since these two sets of data, under our conditions, include junction potentials measurements which are also dependent on Li^+ concentration. From this result, it appears that the V^V/V^{IV} couple in $Na_{0.33}V_2O_5$ behaves as a Nernstian system in the same way that it has been proven for V_2O_5 (10-12).

Therefore, thermodynamic information on insertion compounds $Li_xNa_{0.33}V_2O_5$ can be obtained from EMF temperature measurements of cell A on the basis of the following equations

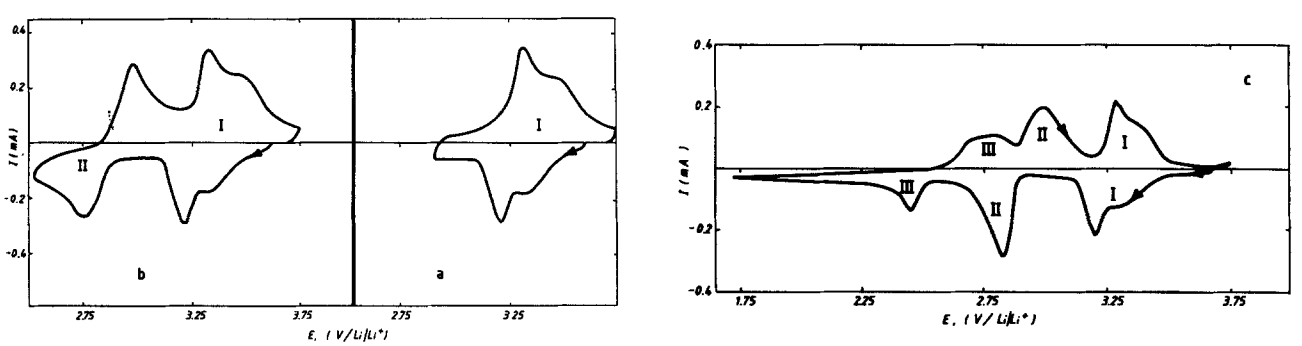

Fig. 1. β $Na_{0.33}V_2O_5$ cyclic voltammetric curves performed between cycling limits of 3.750 and 2.95V (a); 3.75 and 2.50V (b); and 3.75 and 1.75V (c). The scanning speed was $3.3\ 10^{-4}$ V s^{-1} for (a) and (b) and $1.2\ 10^{-4}$ V s^{-1} for (c).

$$\Delta\bar{G}_{\mathrm{Li}(x,T)} = -FE_{(x,T)} \quad [2]$$

$$\Delta\bar{S}_{\mathrm{Li}(x,T)} = F(\delta E/\delta T)_x \quad [3]$$

$$\Delta\bar{H}_{\mathrm{Li}(x,T)} = F[T(\delta E/\delta T)_x - E] \quad [4]$$

where $\Delta\bar{G}_{\mathrm{Li}}$, $\Delta\bar{H}_{\mathrm{Li}}$, and $\Delta\bar{S}_{\mathrm{Li}}$ are the partial molar Gibbs free energy, enthalpy, and entropy of the overall insertion reaction: $Na_{0.33}V_2O_5 + x\mathrm{Li} \leftrightharpoons Li_xNa_{0.33}V_2O_5$, as a function of the degree of reduction x.

The equilibrium potential curve E *vs.* x of the electrode $Li_xNa_{0.33}V_2O_5$ is reported in Fig. 3. Evolution of the molar Gibbs free energy with x is inconsistent with the simple theoretical EMF-x relationship [1]. Taking the high lithium concentration values required during all the intercalation process into account, it can be assumed that energy contributions arising from repulsive coulombic interactions between Li^+ ions should be considered and added to the concentration dependent term in the EMF-x relationship. Electrochemical lithium insertion into the bronze involves three main steps in the potential window 3.5/2.5V as already evidenced in the voltammetric study. These different steps are well separated by two sudden drops in potential for $x = 0.33$ and $x = 0.70$. The voltage and hence the chemical potential of Li change continuously from 3.5 to 3.28V for $0 < x < 0.2$, and then with a lower slope up to $x = 0.3$. The second and the third steps consist of two voltage plateaus at 2.9 and 2.55V for lithium contents corresponding to $0.34 < x < 0.7$ and $0.75 < x < 1.65$, respectively. These experimental data on the β $Na_{0.33}V_2O_5$ synthesized by a sol-gel process are in good agreement with those found by Raistrick on lithiated β sodium and potassium bronzes (13-15) prepared by a solid-state reaction (SSR).

From measurements reported by Popov *et al.* (16, 17) and Zachau-Christiansen *et al.* (8), it can be seen that electrochemical lithium insertion into β $Li_xV_2O_5$ seems to occur at energy levels close to those observed in β $Na_{0.33}V_2O_5$ for the first two processes ($0 < x < 0.7$). However, opposite to these lithium bronzes wherein a lithium mobility has been proven to take place (8, 16-18), the sodium ions of the $Na_{0.33}V_2O_5$ are found to be very stable, even at higher temperature (150°C) (1, 19). Thus, the control of the upper limit voltage should not affect the rechargeability of the sodium vanadium bronze during cycling experiments.

EMF temperature measurements were performed in the temperature range 20°-60°C. Some typical EMF-T curves are shown in Fig. 4 for different x values in $Li_xNa_{0.33}V_2O_5$. Linear variations are observed throughout the whole x range investigated and in almost all cases, the EMF has a positive temperature coefficient. The values of the partial molar entropy of the insertion reaction of Li into $Na_{0.33}V_2O_5$, $\Delta\bar{S}_{\mathrm{Li}}$ obtained from these measurements according to Eq. [3] are shown in Fig. 5. Insofar as lithium insertion only induces a slight contraction of the c parameter (1), *i.e.*, the initial monoclinic structure remains stable practically for the overall composition range $0 < x < 1.7$, it can be assumed that the variations of the molar partial entropy are mainly correlated to the degree of disorder of lithium during Li intercalation. Two set of data appear for $0 < x < 0.28$ and $0.30 < x < 0.65$, which corresponds to the first step located between 3.5 and 2.9V and then to the voltage plateau occurring at 2.9V, respectively. For very low contents, $x < 0.02$, high values of entropy are found which reflect a high degree of disorder of Li, *i.e.*, a high mobility in the host compound as in the case of silver in monoclinic β $Ag_xV_2O_5$ (20) and of lithium in monoclinic β $Li_xV_2O_5$ (16) and in orthorhombic V_2O_5 (10, 21). This is consistent with the behavior exhibited by lithium considered as a solute species dissolved in the $Na_{0.33}V_2O_5$ solvent. Thereafter, $\Delta\bar{S}_{\mathrm{Li}(x)}$ diminishes with further filling of the vacant sites to reach a minimum value for $x \simeq 0.08/0.1$. Beyond $x = 0.1$, from an initial value of 25 J mol^{-1} K^{-1}, $\Delta\bar{S}_{\mathrm{Li}(x)}$ slowly decreases with x up to $x = 0.20$ and then, a sharp entropy change occurs to lead to a minimum value of $x = 0.28$ where a maximum ordering of Li takes place. From $x > 0.3$, a high degree of disorder appears until $x = 0.6$; thereafter, $\Delta\bar{S}_{\mathrm{Li}(x)}$ diminishes which seems to suggest that a new ordering process takes place.

It is interesting to notice that the minima in ΔS_{Li} variations which can be associated with a high degree of order, do not exactly occur at the compositions expected from $\Delta\bar{G}_{\mathrm{Li}}$ measurements, but fall slightly to the left of the sharp drop of potential. Such a phenomenon, as well as important change in $\Delta\bar{S}_{\mathrm{Li}}$ without significant variation in $\Delta\bar{G}_{\mathrm{Li}}$ have been already evidenced in thermodynamic studies on various Li intercalation compounds such as TiS_2 (22, 23), β $Li_xV_2O_5$ (16), V_2O_5 (21), V_6O_{13} (24, 25), and $Li_xV_3O_8$ (26).

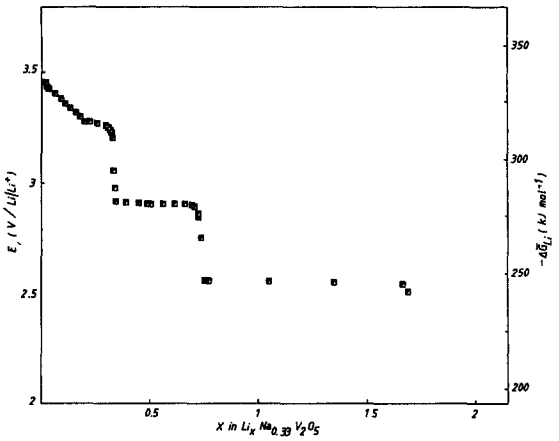

Fig. 3. EMF *vs.* composition curve for electroformed $Li_xNa_{0.33}V_2O_5$ at 20°C.

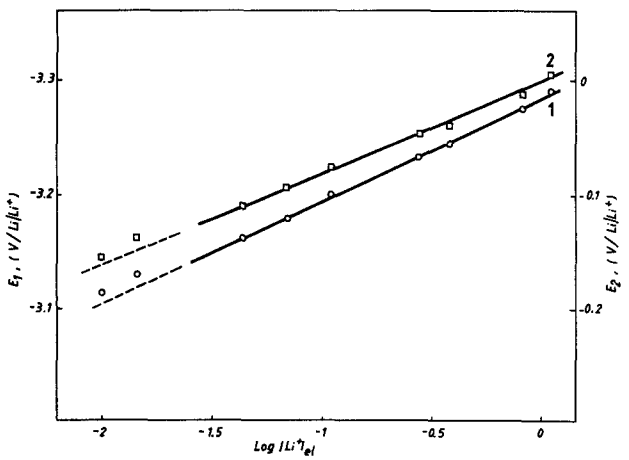

Fig. 2. Variation of potential of a $Li_{0.2}Na_{0.33}V_2O_5$ electrode (1) and a lithium electrode (2) as a function of Li^+ concentration in electrolyte at 20°C. Potential variations of both electrodes were simultaneously recorded in same cell *vs.* same reference electrode.

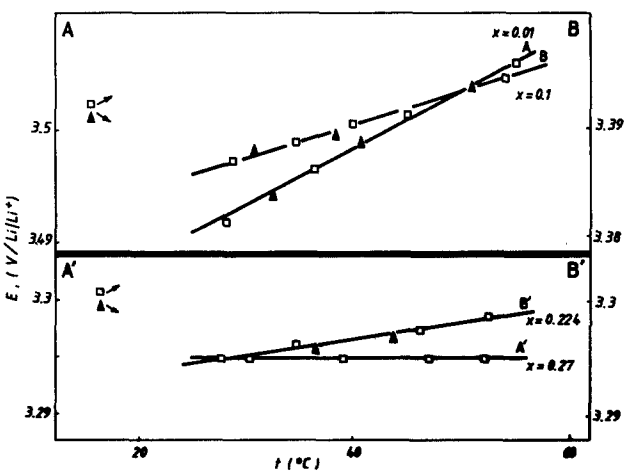

Fig. 4. EMF-temperature behavior of the Li/1M $LiClO_4$ in PC/$Li_xNa_{0.33}V_2O_5$ cell (T = 20°-60°C).

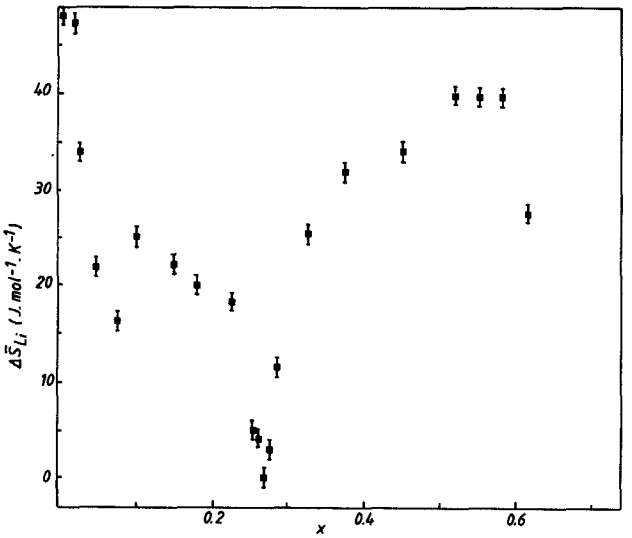

Fig. 5. Partial molar entropy of lithium as a function of x in $Li_xNa_{0.33}V_2O_5$.

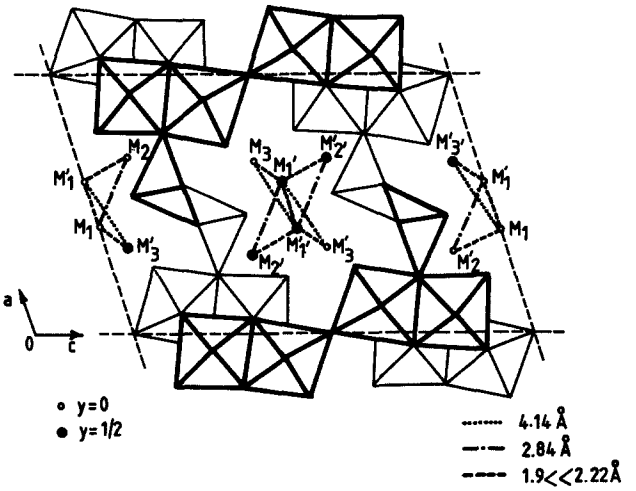

Fig. 7. Projection of the crystal structure of β $Na_{0.33}V_2O_5$ on the ac plane and possible positions of the inserted cations [adapted from Ref. (29, 30)]. The distance M-M for the three different sites were calculated in a previous work (1).

From the experimental data $\Delta\bar{S}_{Li}$ and from the potential variation E *vs* x, using Eq. [4], the partial molar enthalpy of insertion of Li in $Na_{0.33}V_2O_5$ is determined at 20°C as a function of x (Fig. 6). This molar function mainly reflects the Li strong bonding to the bronze structure; at the same time, $\Delta\bar{H}_{Li}$ includes an opposite contribution related with the interaction energy arising from the repulsive interactions between the inserted alkali ions. The main feature in $\Delta\bar{H}_{Li}$ variations consists of two distinct sets of data for the lithium contents $0 < x < 0.3$ and $0.3 < x < 0.65$. For each insertion process, $\Delta\bar{H}_{Li}$ is quite constant which confirms the equivalence of the concerned sites. Other electrochemical determinations of $\Delta\bar{H}_{Li}$ for lithium insertion in monoclinic β $Li_xV_2O_5$ are in line with our data (16). For high lithium contents ($x > 0.3$), the lower values of Li bonding to the bronze structure can be explained by an increase in contribution of coulombic interactions to $\Delta\bar{H}_{Li}$. No calorimetrically determined $\Delta\bar{H}_{Li}$ for Li insertion into $Na_{0.33}V_2O_5$ are presently available, but our results are consistent with enthalpies of formation of sodium vanadium bronzes given by Dickens *et al.* (27).

The tunnel structure of the β $Na_{0.33}V_2O_5$ bronze (Fig. 7) contains three types of sites called M_1, M_2, M_3 which correspond, respectively, to four tetrahedral, four eight coordinated, and from octahedral sites per unit cell ($M_{12}V_{12}O_{30}$) (6, 28-30). Taking into account the half occupancy of the M_1 sites by sodium ions in the initial material $Na_2V_{12}O_{30}$ and the fact that the filling of sites is all the more easy because the distances between are already occupied sites and a vacant site is large, calculation for the M-M distances (1) allows us to suggest that the first two processes could correspond to the half occupancy of the M_3 sites filled between 3.5 and 2.9V and of the M_2 sites at 2.9V. The subsequent lithium insertion occurring at about 2.55V can be understood insofar as the distance between filled and vacant sites corresponding to a mean value of about 2Å (from 1.9 up to 2.2Å), the accessibility of all the vacant sites is then practically similar. Therefore, Li^+ ions in the concentration range $0.6 < x < 1.7$ are accommodated in the bronze structure in half of all the remaining sites at a same energy level. The evolutions of all the molar partial functions $\Delta\bar{S}_{Li}$, $\Delta\bar{H}_{Li}$, $\Delta\bar{G}_{Li}$ *vs.* x are in accordance with, and confirm the previous scheme proposed (1) to explain the electrochemical behavior of the β $Na_{0.33}V_2O_5$ bronze in terms of crystallographic data. Although the splitting of the first step into two processes, as evidenced in voltammetric and chronopotentiometric curves (1, 8), has been confirmed by our thermodynamic investigations, only additional energetic and structural information could elucidate this phenomenon.

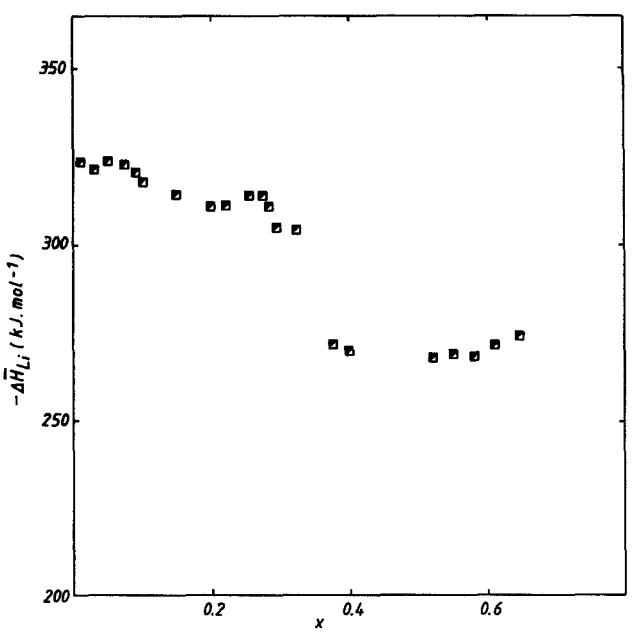

Fig. 6. Partial molar enthalpy of lithium as a function of x in $Li_xNa_{0.33}V_2O_5$.

Kinetics

In a previous work, we have proven that the cycling behavior of the β $Na_{0.33}V_2O_5$ bronze synthesized by a sol-gel process was strongly improved as compared with that exhibited by the bronze of similar formula, prepared by a solid-state reaction at high temperature (SSR bronze). Since the sol-gel technique yields to a bronze wherein all the tunnels of the structure are aligned over larger domains parallel to the *a-b* plane, we had concluded that improvement for the diffusion of Li^+ ions in the SGP bronze could be explained in terms of structural anisotropy. Hence kinetics measurements are of the utmost importance since the current density which this cathodic material will be able to sustain without significant overvoltage will depend on the diffusion of Li^+ ions in the tunnel structure of the bronze.

The influence of the current density on the discharge curves of the SGP bronze $Na_{0.33}V_2O_5$ is reported in Fig. 8. The decrease in the total faradaic yield is especially ascribed to the third step (2.55V) and then to the second one, whereas the first process requiring the insertion of about 0.3 Li^+ per mole of bronze is never significantly affected.

Chemical diffusion coefficients measurements were performed using the current pulse relaxation technique described by Basu and Worrel (31). A negligible amount of lithium is introduced at the interface of the working elec-

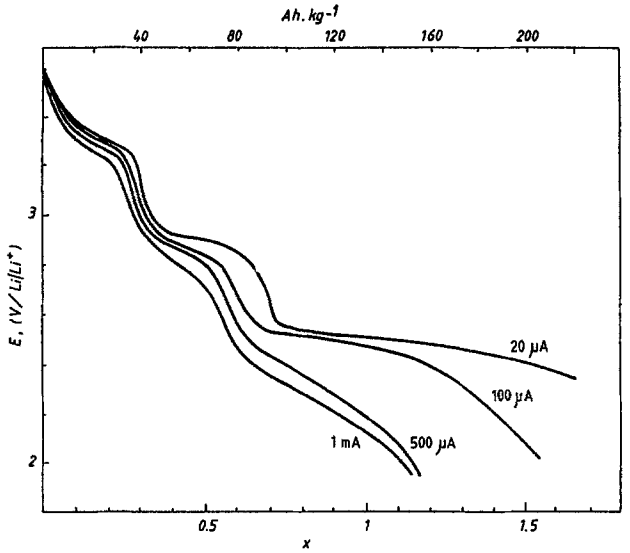

Fig. 8. Influence of the current density on the chronopotentiometric curves for the reduction of the β $Na_{0.33}V_2O_5$ bronze in 1M $LiClO_4$ solution in PC at 20°C.

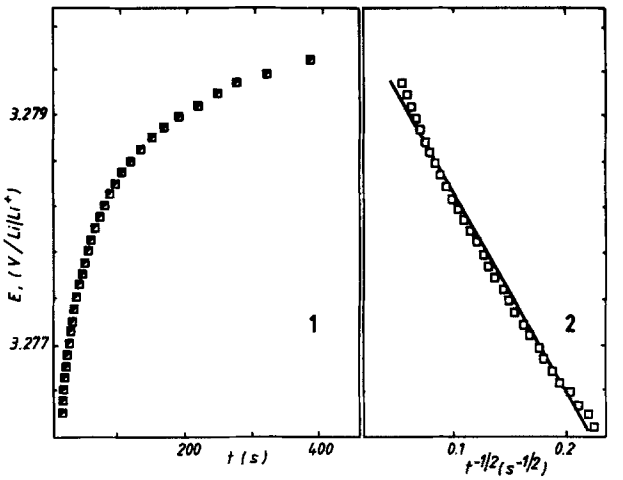

Fig. 9. Typical voltage-time relations during equilibration of the cell voltage after a negligible amount of lithium is introduced in $Li_xNa_{0.33}V_2O_5$ by a short constant current pulse. $x = 0.25$; $i = 0.240$ mA; $\tau = 30$s; $A = 0.64$ cm^2.

trode (90% by weight graphite) by a short current pulse inducing a decrease of the voltage from its previous equilibrium value. After the current is switched off, the cell voltage increases to an equilibrium value close to the previous one. Thus, the rate of diffusion of lithium into the bulk of the cathodic material would control the equilibration rate of the cell voltage.

Fick's second equation for an instantaneous planar source of diffusing species in semi-infinite geometry yields to the evolution of the relaxation potential as a function of $t^{-1/2}$, from which, the chemical diffusion coefficient $\tilde{D}_{Li}$ is calculated according to Eq. [5]

$$\tilde{D}_{Li} = \left[\frac{i\tau V_m}{A\mathbf{F}\pi^{1/2}}(dE/dx)(dE/dt^{-1/2})^{-1}\right]^2 \quad \text{if } t << L^2/\tilde{D}_{Li} \quad [5]$$

where i, τ, V_m, A, $\mathbf{F}$, t, and L are, respectively, the current pulse (A), the pulse duration(s), the molar volume (55.3 cm^3/mol), the geometric area (cm^2) corresponding to the SGP β $Na_{0.33}V_2O_5$ platelets, *i.e.*, to the pure cathodic material (≃2 mg) or to the grains (≃20/30 μm in diam) of the SSR bronze, the Faraday constant, the time(s), and the half-thickness of the material since the electrolyte is in contact with both sides of the sample. (dE/dx) and $(dE/dt^{-1/2})$ are the local slope of the equilibrium potential composition curve and the slope of the straight line obtained from the evolution of the relaxation potential *vs.* $t^{-1/2}$. The current pulses used are in the range 0.2/0.4 mA and pulse duration between 10 and 20s. The consistency of these determinations has been checked by performing similar experiments for several x values but with different values for A, i, and τ.

The time potential dependence after pulse interruption and the corresponding potential $-t^{-1/2}$ relation for a typical experiment are shown in Fig. 9. Experimental data found for the chemical diffusion coefficient of Li^+ ions, as a function of x in $Na_{0.33}V_2O_5$ prepared via a sol-gel process, are summarized in Table I. Three sets of data of different order of magnitude are pointed out and related to three distinct composition ranges which reflects that Li accommodation in the SGP bronze takes place in three different types of sites.

Moreover, it can be seen that $\tilde{D}_{Li}$ decreases as the lithium content in the bronze increases. Thus, for each process, D_{Li} seems to be proportional to the fractional number of vacant sites, assuming all sites have an equal probability of being occupied as suggested in our explanation of the different energy levels for Li incorporation. For $0 < x < 0.7$, $\tilde{D}_{Li}$ varies from 10^{-9} up to 10^{-12} cm^2 s^{-1}. In fact, these values are of the same order of magnitude as those found for lithium in orthorhombic $Li_xV_2O_5$ at room temperature (32) whereas other works on Li diffusion in β $Li_xV_2O_5$ give conflicting data for $\tilde{D}_{Li}$ in the range 10^{-11}-10^{-12} cm^2 s^{-1} for $0 < x < 1.3$ (8) and 10^{-13} cm^2 s^{-1} for $x = 0.28$ (17). Generally, Li diffusion in vanadium oxides ranked among the most promising rechargeable cathodic materials such as V_6O_{13} and $Li_{1+x}V_3O_8$ gives rise to high values in the range 10^{-8}-10^{-10} cm^2 s^{-1}. The value of $\tilde{D}_{Li}$ $8 \cdot 10^{-14}$ cm^2 s^{-1} found for $x = 0.8$, which is many orders of magnitude lower than that obtained for the first two steps, is consistent with the strong influence of the current density on the discharge curves (Fig. 8) and the results of the voltammetric study, since only the third step occurring at 2.55V is found to be significantly involved in the decrease of the electrochemical performances of the cathodic material.

The typical strong decrease of $\tilde{D}_{Li}$ as the lithium content in $Li_xNa_{0.33}V_2O_5$ increases all along the composition range $0 < x < 1.65$ can be explained by the nature of the host lattice involved in the lithium intercalation process. Indeed, our preliminary investigations about the determination of structural parameters for various x values have shown besides that the initial monoclinic β structure was stable. Now, it is well known that Li insertion in Van der Waals bonded compounds such as TiS_2 (22, 31) and MoO_3 (33, 34) or in layered-like oxides such as V_2O_5 (35, 37), occurs with a separation of the layers inducing a continuous expansion of the lattice and the emergence of new phases which implies that $\tilde{D}_{Li}$ is constant, or increases or decreases at the most one-order of magnitude in a wide concentration range. In contrast, the stable and rigid three-dimensional tunnel structure of the bronze, probably hinders any important structural change which explains that $\tilde{D}_{Li}$ always falls with further Li insertion.

Determination of the thermodynamic factor, discussed by Weppner and Huggins (38) in the case where the sample

Table I. Variation of the chemical ($\tilde{D}_{Li}$) and component diffusion coefficient of lithium (D_K) as a function of x in $Li_xNa_{0.33}V_2O_5$

	SGP[a] bronze		SSR[b] bronze
x	$\tilde{D}_{Li}$ (cm^2 s^{-1})	D_K (cm^2 s^{-1})	$\tilde{D}_{Li}$ (cm^2 s^{-1})
0.025	$7 \cdot 10^{-9}$	10^{-8}	$7 \cdot 10^{-11}$
0.075	—	—	$4 \cdot 10^{-11}$
0.10	$4.4 \cdot 10^{-8}$	$4 \cdot 10^{-8}$	$7 \cdot 10^{-10}$
0.20	—	—	$2.6 \cdot 10^{-11}$
0.25	$4 \cdot 10^{-10}$	$2 \cdot 10^{-10}$	—
0.30	$4.3 \cdot 10^{-12}$	$2 \cdot 10^{-12}$	—
0.40	$1 \cdot 10^{-11}$	$6 \cdot 10^{-11}$	$8 \cdot 10^{-14}$
0.50	$2.3 \cdot 10^{-12}$	$2.5 \cdot 10^{-12}$	—
0.80	$8 \cdot 10^{-14}$	10^{-13}	—

[a] $A = 0.64$ cm^2
[b] $A = 2.2$ cm^2

Table II. Variation of the partial ionic conductivity σ_{Li} as a function of the lithium content x in $Li_xNa_{0.33}V_2O_5$

x	0.025	$0 \cdot 10$	0.25	0.30	0.40	0.50	0.80
$\sigma_{Li}(\Omega^{-1}\,cm^{-1})$	$1.3 \cdot 10^{-5}$	$8.3 \cdot 10^{-5}$	$3.5 \cdot 10^{-6}$	$4 \cdot 10^{-8}$	$4 \cdot 10^{-7}$	$9 \cdot 10^{-8}$	$7 \cdot 10^{-9}$

is predominantly an electronic conductor, provides an evaluation of the influence of the transport of charges species (e^-, Li^+) upon each other in the studied bronze $Li_xNa_{0.33}V_2O_5$. With the molar volume changing by only 2% when $0 < x < 1.6$ (1), the thermodynamic factor may be evaluated from the present experiments according to $W = -x(F/RT)(dE/dx)$ (34). The compositional variation of the thermodynamic factor is reported in Fig. 10. W is seen to increase with x for each process but decreases through the whole concentration range to reach a mean value, close to unity, independent of x for the second and the third voltage plateau. The component diffusion coefficient $D_{K(Li)}$ related to the chemical diffusion coefficient following the relationship $\tilde{D}_{Li} = WD_{K(Li)}$ (34) is a measure of the random motion of Li in the crystal framework and depends on Li concentration as reported in Table I. The thermodynamic factor may be combined with data for the component diffusion coefficient in order to obtain the partial lithium ion conductivity σ_{Li} whose values determined from the relation

$$\sigma_{Li} = \frac{F\tilde{D}_{Li}}{Vm}\left(\frac{dE}{dx}\right)^{-1}$$

are summarized in Table II.

Additional kinetic measurements were performed on the β $Na_{0.33}V_2O_5$, prepared by the usual solid-state reaction at 650°C. Comparison of $\tilde{D}_{Li}$ *vs.* x for both SSR and SGP bronzes (Table I) clearly emphasizes that lithium transport is one-hundred fold faster in the anisotropic structure whatever the lithium content. Such a feature is consistent with the alignment of the tunnels parallel to each other over larger domains in SGP bronze, which explains the better electrochemical behavior observed for this latter as compared to that exhibited by the SSR bronze (1).

Conclusion

The thermodynamic and kinetic data obtained have allowed us to explain the electrochemical lithium intercalation process in the sodium vanadium bronze β $Na_{0.33}V_2O_5$.

In the composition ranges $0 < x < 0.3$ and $0.3 < x < 0.7$ in $Li_xNa_{0.33}V_2O_5$, two main ordering processes are seen to take place; they are consistent with the scheme previously suggested (1) to describe the filling of the available sites M of the β structure by Li^+ ions.

From a kinetic viewpoint, determination of the chemical diffusion coefficient $\tilde{D}_{Li}$ of lithium in the SGP bronze as a function of x has shown that $\tilde{D}_{Li}$ decreases for each process and all along the x composition range, i.e., $\tilde{D}_{Li}$ is found to be proportional to the fractional number of vacant sites. $\tilde{D}_{Li}$ varies from 10^{-9} up to 10^{-12} $cm^2\,s^{-1}$ for $0 < x < 0.7$ whereas lower values in the order 10^{-14} $cm^2\,s^{-1}$ are found for higher lithium contents ($x > 0.7$).

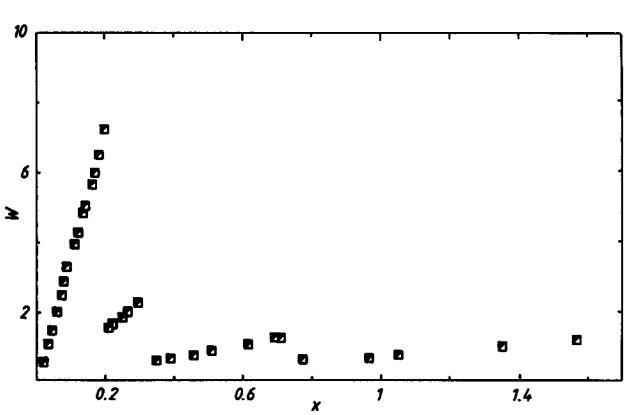

Fig. 10. Compositional variation of the thermodynamic factor

Moreover, a comparative study of $\tilde{D}_{Li}$ in both SGP and SSR bronzes has again highlighted the advantage of the sol-gel technique which enables the strong enhancement of the structural anisotropy of the $Na_{0.33}V_2O_5$ bronze and the diffusion of Li^+ ions in the tunnel structure of the host lattice.

This work reveals that the electrochemical performance of an intercalation compound is significantly dependent on the method used for its synthesis. Therefore, the sol-gel technique should be considered with utmost interest for the preparation of new promising cathodic intercalation materials usable in secondary Li cells.

Acknowledgments

The financial support by the Direction des Recherches, Etudes et Techniques (D.R.E.T., Décision no. 86186) is gratefully acknowledged.

Manuscript submitted April 14, 1989; revised manuscript received Sept. 5, 1989.

Laboratoire d'Electrochimie Catalyse et Synthese Organique, CNRS, assisted in meeting the publication costs of this article.

REFERENCES

1. J. P. Pereira-Ramos, R. Messina, L. Znaidi, and N. Baffier, *Solid State Ionics*, **28-30,** 886 (1988).
2. J. J. Legendre and J. Livage, *J. Colloid Interface Sci.*, **94,** 75 (1983).
3. P. Aldebert, N. Baffier, N. Gharbi, and J. Livage, *Mater. Res. Bull.*, **16,** 669 (1981).
4. A. Bouhaouss, P. Aldebert, N. Baffier, and J. Livage, *Rev. Chim. Min.*, **22,** 17 (1985).
5. L. Znaidi, D. Lemordant, and N. Baffier, *Solid State Ionics*, **28-30,** 1750 (1988).
6. A. D. Wadsley, *Acta Cryst.*, **8,** 695 (1955).
7. J. P. Gabano, M. Broussely, J. P. Pereira-Ramos, R. Messina, and J. Perichon, Fr. Pat. 15,082 (1985).
8. B. Zachau-Christiansen, K. West, and J. Jacobsen, *Solid State Ionics*, **9-10,** 399 (1983).
9. F. W. Lytle, R. B. Greegor, and I. D. Raistrick, *J. Phys.*, **C8,** 47, 719 (1986).
10. J. P. Pereira-Ramos, Thése de Doctorat d'Etat, Paris (1988).
11. J. P. Pereira-Ramos, R. Messina, C. Piolet, and J. Devynck, *J. Power Sources.*, **20,** 221 (1987).
12. M. V. Ptitsyn, K. I. Tikhonov, and A. L. Rotinyan, *Elektrokhimiya*, **18,** 1556 (1982).
13. I. D. Raistrick, *Solid State Ionics*, **9-10,** 425 (1983).
14. I. D. Raistrick and R. A. Huggins, *Mater. Res. Bull.*, **18,** 337 (1983).
15. I. D. Raistrick, *Rev. Chim. Min.*, **21,** 456 (1984).
16. A. V. Popov, Yu. G. Metlin, and Yu. D. Tretyakov, *J. Solid State Chem.*, **32,** 343 (1980).
17. Yu. D. Tretyakov, A. V. Popov, and Yu. D. Metlin, *Solid State Ionics*, **17,** 265 (1985).
18. J. Gendell, R. M. Cotts, and M. J. Sienko, *J. Chem. Phys.*, **37,** 220 (1962).
19. B. C. H. Steele, in "Mass Transport Phenomena in Ceramics," A. R. Cooper and A. H. Hener, Editors, p. 269, Plenum Press, New York (1975).
20. B. B. Scholtens, R. Polder, and G. H. J. Broers, *Electrochim. Acta*, **23,** 483 (1978).
21. J. P. Pereira-Ramos, R. Messina, C. Piolet, and J. Devynck, *ibid.*, **33,** 1003 (1988).
22. A. H. Thompson and C. R. Symon, *Solid State Ionics*, **3-4,** 175 (1981).
23. A. H. Thompson, *Physica*, **105B** 461 (1981); *This Journal*, **126,** 608 (1979).
24. P. C. Spurdens, J. Drennan, J. R. Owen, B. C. H. Steele, J. M. Gonzales-Calbet, and D. A. Jefferson, *Solid State Ionics*, **5,** 335 (1981).
25. P. C. Spurdens and B. C. H. Steele, *ibid.*, **21,** 151 (1986).

26. G. Pistoia, M. L. Di Vona, and P. Tagliatesta, *ibid.*, **24,** 103 (1987).
27. P. G. Dickens, M. Jewess, D. J. Neil, and J. C. W. Rose, *J. Chem. Soc. Dalton Trans.*, 30 (1973).
28. H. Kobayashi, *Bull Chem. Soc. Jpn.*, **52,** 1315 (1979).
29. J. Galy, J. Darriet, A. Casalot, and J. B. Goodenough, *J. Solid State Chem.*, **1,** 339 (1970).
30. T. Erata, *J. Chem. Soc. Jpn.*, **36,** 297 (1981).
31. S. Basu and W. L. Worrel, in "Fast Ion Transport in Solids," Vashita, Mundy, and Shenoy, Editors, p. 149, Elsevier, North Holland (1979).
32. J. Farcy and R. Messina, *This Journal,* In press.
33. M. Pasquali, G. Pistoia, and F. Rodante, *Solid State Ionics,* **6,** 319 (1982).
34. J. O. Besenhard and R. Schollhorn, *J. Power Sources,* **1,** 267 (1976/1977).
35. D. W. Murphy, P. A. Christian, F. J. Di Salvo, and J. V. Waszczak, *Inorg. Chem.*, **18,** 2800 (1979).
36. Y. Muranushi, T. Miura, T. Kishi, and T. Nagai, *J. Power Sources,* **20,** 187 (1987).
37. P. G. Dickens, S. J. French, A. T. Hight, and M. F. Pye, *Mater. Res. Bull.*, **14,** 1295 (1979).
38. W. Weppner and R. A. Huggins, *This Journal,* **124,** 1569 (1977).

Rapid Determination of Corrosion Chamber Uniformity

Rudolf Schubert and Glen G. Neuburger

Bell Communications Research, Red Bank, New Jersey 07701

ABSTRACT

Intra- and interlaboratory comparison of the results obtained with flowing mixed gas accelerated atmospheric corrosion chambers (FMG-AACC) suggests nonuniform conditions for corrosion studies. In this paper we present the use of strategically positioned quartz crystal microbalances (QCM) to rapidly determine, *in situ*, spatial uniformity in a FMG-AACC. It is further demonstrated that localized chamber overloading, undetected by measurement of exhaust pollutant gas concentrations, can be monitored with the aid of a QCM. Corrosion film thicknesses are confirmed by Auger electron spectroscopy and sputter ion depth profiling.

Accelerated atmospheric corrosion chambers (AACC) are coming into widespread use as more standards writing organizations are addressing the need for controlled accelerated corrosion testing.[1] Recent studies have demonstrated the necessity for use of flowing mixed gas (FMG) corrosion chambers with control and concentration verification of all pollutant gases (1). Chambers with a variety of configurations and sizes, gas exchange rates, and corrosion environments have been presented (1-5). Interlaboratory comparison of the results obtained for corrosion of metals utilizing a wide variety of FMG-AACC suggests nonuniform conditions for corrosion studies, even for systems with verification of pollutant gas concentration. Intralaboratory comparison of corrosion data suggests the nonuniform distribution of pollutant gases within the corrosion chamber. With the utilization of highly surface reactive gases, such as chlorine or hydrogen chloride, it is imperative that the air flow and pollutant concentration throughout the FMG-AACC be spatially uniform with reproducible concentrations if one is to achieve consistent results. The lack of reproducibility or point-to-point spatial uniformity within a single FMG-AACC makes the interlaboratory comparison of many FMG-AACC difficult and meaningless.

Previous methods for standardization of corrosion rates have been based primarily on gravimetric measurements of metallic coupons removed from the FMG-AACC; this is the present method listed for several standards already in existence. This method suffers, however, from the long exposure times necessary to make an accurate assessment of the corrosion rate. For example, a corrosion film growth rate of 50 Å/h (density = 1 g/cm^3), which corresponds to 0.5 μg/h/cm^2, would require an exposure time of approximately 100h to measure the corrosion rate with an error of <10%. Gravimetric methods, involving post- or interrupted exposure measurements, also suffer from the inability to continuously monitor corrosion rates during the entire exposure. Cathodic reduction (6) has been used as an alternative method for measuring corrosion film growth; however, the irreversible nature of this measurement does not lend itself to ongoing corrosion rate measurements. Electron microscopy coupled with energy dispersive x-ray analysis can provide a rapid estimation of corrosion rates, however, corrosion film thicknesses of 100-1000Å are needed for analysis and the sensitivity to oxides is poor. Sputter depth profiling (7, 8) coupled with any of several surface analytical techniques (*e.g.*, Auger electron or x-ray photoelectron spectroscopy) provides a means for approximating the corrosion film thickness, but the long analysis time in conjunction with the high cost per analysis has excluded its use for routine measurements.

Previously, Schubert (5) presented a FMG-AACC which utilizes dynamic, continuous, *in situ* monitoring of weight gain on surfaces of similar elemental composition to those surfaces being tested during exposure. This system utilizes four quartz crystal microbalances (QCM) placed within the FMG-AACC. Despite its obvious advantages (9), QCM have been utilized in only a few corrosion studies (5, 10, 11) although schemes which utilize QCM for gas detection have been known for over two decades (12).

Techniques employing QCM rely on the decrease in resonant frequency of the quartz crystal with an increase in mass loading; that is

$$\Delta F = \frac{-2F^2}{p_q v_q} \Delta m/A \qquad [1]$$

where, ΔF is the change in frequency (Hz) as a result of mass loading; F is the resonant frequency of the quartz crystal (Hz); p_q is the density of the quartz (kg/m^3); v_q is the shear wave velocity (m/s); and $\Delta m/A$ is the change in areal density (kg/m^2). This latter quantity may be rewritten as $p_f t_f$ and the film thickness, t_f, can be calculated if the density, p_f, is known. For AT-cut quartz, p_q 2648 kg/m^3 and v_q = 3340 m/s (9), and Eq. [1] takes the form

$$\Delta F = -2.3 \times 10^6 F^2 \Delta m/A \qquad [2]$$

where, ΔF, F, and $\Delta m/A$ are expressed in units of Hz, MHz, and g/cm^2, respectively. With present day instrumentation, frequencies can easily be measured with a precision of <1 Hz, thus allowing areal density determinations of 10^{-9} g/cm^2 or less.

In this paper we describe the use of strategically positioned QCMs to determine, *in situ*, FMG-AACC spatial nonuniformity in a chamber which was expected to have a spatially uniform gas distribution since the pollutant gas inlet/outlet was distributed over the chamber volume (5). Confirmation of variations in spatial uniformity is demon-

[1] Standards for various types of atmospheric corrosion testing have already been implemented or are being considered by the ASTM, DIN (Germany), IEC, IEEE, ISA, ISO, JEIDA, SSG (Sweden), and possibly NACE.